Volume 1
Number 2
May 2020
Pages 111–282

Materials Advances

rsc.li/materials-advances

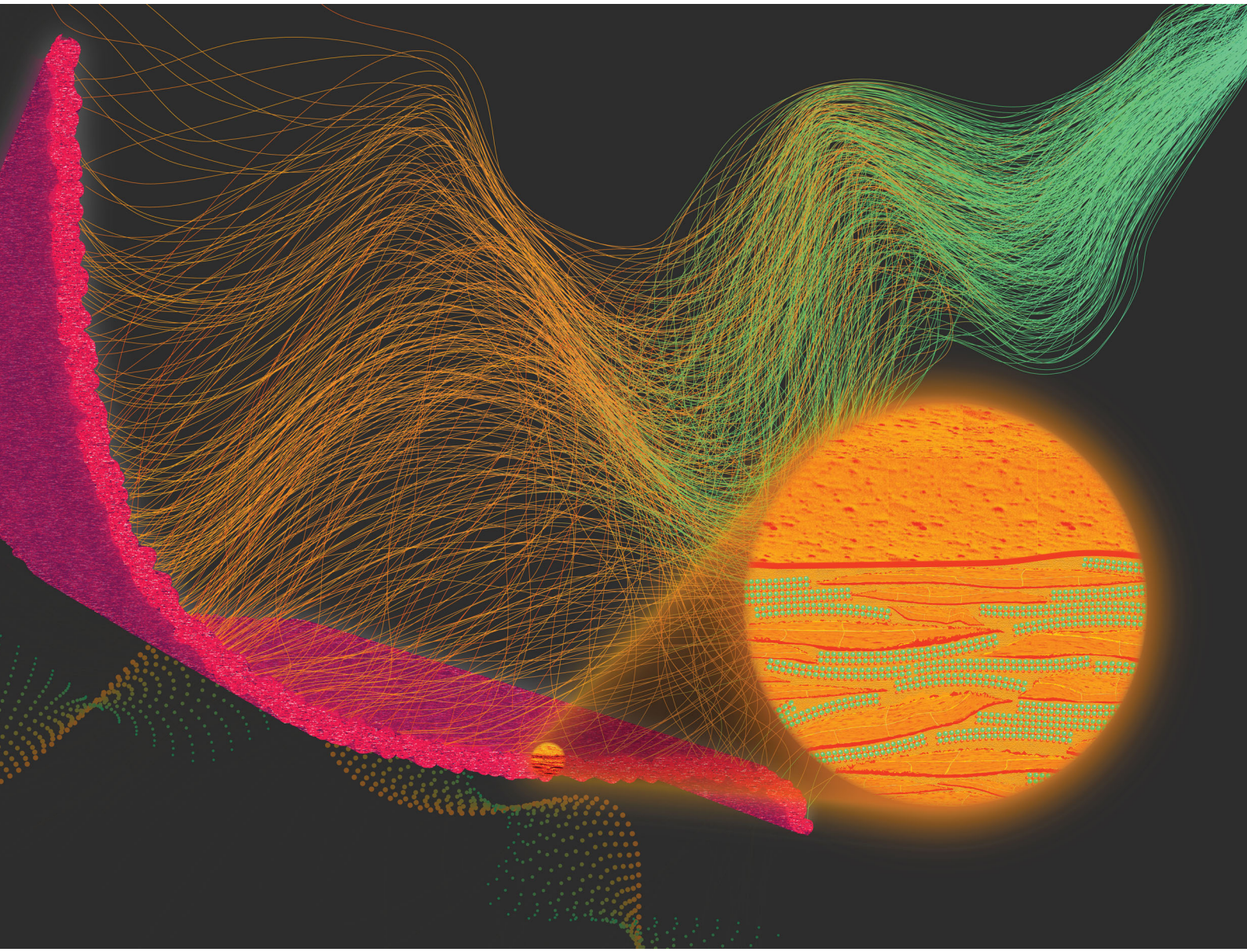

ISSN 2633-5409

ROYAL SOCIETY OF CHEMISTRY

PAPER

Praveen C. Ramamurthy, Daniel Q. Tan *et al.*
MXene interlayered crosslinked conducting polymer film for highly specific absorption and electromagnetic interference shielding

Materials Advances

ROYAL SOCIETY OF CHEMISTRY

PAPER

View Article Online
View Journal | View Issue

Cite this: *Mater. Adv.*, 2020, **1**, 177

MXene interlayered crosslinked conducting polymer film for highly specific absorption and electromagnetic interference shielding†

Pritom J. Bora, ‡[a] Amith G. Anil,‡[b] Praveen C. Ramamurthy*[b] and Daniel Q. Tan *[a]

In this work, the electromagnetic interference (EMI) shielding properties of an MXene interlayered crosslinked conducting poly(3,4-ethylenedioxythiophene):poly(styrene sulfonate) (PEDOT:PSS) polymer film are investigated. The introduction of a crosslinker into PEDOT:PSS makes PEDOT:PSS water insoluble. An average EMI shielding effectiveness (SE) of ~41 dB (corresponding to 99.999% blockage) was obtained for a solution coated 6 ± 0.2 μm thick optimized crosslinked PEDOT:PSS-$Ti_3C_2T_x$ MXene (XPM50) nanocomposite film. Electrodynamic modelling and simulation also suggest an excellent SE for this nanocomposite system. From an application point of view, the specific EMI SE (SSE)/thickness (*t*) or absolute EMI SE is the most useful factor. The absolute EMI SE of the XPM50 film is observed to be 89 924 dB cm^2 g^{-1}, which is nearly nine times higher than that of the pristine PEDOT:PSS film and more than three times higher than that of the $Ti_3C_2T_x$ MXene film. Mechanistically, the superior EMI shielding due to absorption (SE_A) is intrinsically predominant. The crosslinked PEDOT:PSS interconnects with the $Ti_3C_2T_x$ MXene flakes, generating more absorption sites and enhanced electrical conductivity which is responsible for the high SE_A value. The XPM50 film also fulfils many commercial requirements, especially solution processability and outstanding absolute EMI SE, which makes it an attractive EMI shield for real time applications such as telecommunications, health care systems, detective systems, defence, and aerospace applications.

Received 6th February 2020,
Accepted 12th April 2020

DOI: 10.1039/d0ma00005a

rsc.li/materials-advances

Introduction

In recent years, electromagnetic disruption (electromagnetic interference or EMI) has become a serious issue for telecommunications,[1] health care systems,[1,2] detective systems,[3] military applications,[4] aerospace applications,[3,4] *etc.*, as it affects the normal function of sensitive apparatus/systems.[4] Moreover, EMI can also take place within electromagnetic organs such as the heart and thus becomes dangerous to human health.[5] Nowadays, electromagnetic protection clothes are preferred for pregnant women, the electronics industry, medicine, and the military.[6] Present technology demands coatable, corrosion protective, water-insoluble, ultra-light, thin, solution-processable, and flexible EMI shields with a high absorption predominant shielding effectiveness (for practical applications, the EMI shielding effectiveness or SE should be ~30 dB which corresponds to 99.99% shielding).[1,4,7]

Traditionally, metals and alloys have been used for EMI shielding, however, due to their many disadvantages such as their susceptibility to corrosion and oxidation, high density, chemical resistance, and difficult processability, some other carbon-based materials are preferred.[7–10] Carbon black (CB), carbon fibers (CFs), carbon nanotubes (CNTs), and reduced graphene oxide (rGO) have been used as fillers in different non-conducting polymer matrices for EMI shielding applications, as the composites possess tunable electrical conductivities which is an intrinsically important factor for EMI shielding along with composite design.[8,9] Recently, a new family of 2D nanomaterials, 2D transition metal carbides (MXenes), and their impregnation into polymers (SA) were reported for EMI shielding with a maximum EMI SE of ~90 dB for a thickness of 45 μm.[1] MXenes have attracted interest for EMI shielding due to their intrinsic properties such as conductivity and surface-rich functional groups.[1] Moreover, MXenes exhibit excellent specific EMI SE and absolute EMI SE.[1] Highly conducting 2D MXenes with multilayer features are desirable for absorption predominant shielding, wherein the

[a] *Department of Materials Science and Engineering, Technion Israel Institute of Technology and Guangdong Technion Israel Institute of Technology, Shantou, Guangdong Province, 515063, China. E-mail: daniel.tan@gtiit.edu.cn, onegroupb203@gmail.com*

[b] *Department of Materials Engineering, Indian Institute of Science, Bangalore 560012, India*

† Electronic supplementary information (ESI) available. See DOI: 10.1039/d0ma00005a

‡ Contributions of both authors are equal.

numerous inter-layers provide a difficult path for incident electromagnetic waves.[1,6] In addition, MXenes exhibit high dielectric loss in solution-processable polymer matrices at a low percolation limit, showing promise as ultra-light EMI shields. Among the different MXenes, the $Ti_3C_2T_x$ (T_x denotes surface-terminating functional groups such as F, O, and OH) MXene has received tremendous attraction because of its better electronic properties.[1] Lately, Liu *et al.* reported a lightweight MXene foam for EMI shielding.[3] Similarly, Bian *et al.* reported MXene aerogel for EMI shielding.[7] $Ti_3C_2T_x$ MXene loaded polymer nanocomposites have been proposed as absorption predominant EMI shields by various research groups.[1,6,11–13] Wang *et al.* studied epoxy-$Ti_3C_2T_x$ MXene nanocomposites for EMI shielding. According to their study, a maximum EMI SE of ~30 dB could be achieved for a thickness of 2 mm. However, the SE increased to ~40 dB for the same thickness after heat treatment.[11] Modern digital systems require coatable thin polymer nanocomposites (films) with excellent absorption predominant EMI SE values.[4] Intrinsically conducting polymers (ICPs) such as polyaniline (PANI) nanocomposite films are well-known for EMI shielding as the matrix itself could provide absorption predominant EMI shielding.[14–16] Zhang *et al.* synthesized co-doped PANI-$Ti_3C_2T_x$ MXene nanocomposites and investigated the EMI shielding properties.[17] They reported an EMI SE value of ~37 dB for a 40 μm thick PANI-$Ti_3C_2T_x$ MXene nanocomposite film.[17] However, maintaining the conductivity and stability of PANI is a challenge because it is de-doped over time.[4] Recently, among the conducting polymers, poly(3,4-ethylenedioxythiophene):poly(styrene sulfonate) (PEDOT:PSS) has drawn special attention due to its facile processability and tunable conductivity.[4] However, our understanding of the EMI shielding properties of PEDOT:PSS films is very limited, which is believed to be due to its water-soluble nature. Li *et al.* studied the EMI shielding properties of a polyurethane-PEDOT:PSS blend, and reported that an EMI SE of ~70 dB was achievable for a 0.15 mm thick PU-PEDOT:PSS blend.[18] Liu *et al.* studied the EMI shielding properties of a PEDOT:PSS-$Ti_3C_2T_x$ MXene film. An EMI SE of ~40 dB was reported for the PEDOT:PSS-$Ti_3C_2T_x$ MXene film (10 μm) in the X-band (8.2–12.4 GHz).[19] However, PEDOT:PSS stand-alone thin films exhibit high moisture sensitivity and thus are not suitable for real time EMI shielding applications. Recently, Mantione *et al.* reported a crosslinking method to make moisture resistant PEDOT:PSS free-standing films.[20] Here the crosslinker acts as the dopant and improves the electronic properties of the films. So far, MXene interlayered conducting polymer (PEDOT:PSS, PANI, *etc.*) films for EMI shielding have been studied.[19] However, crosslinked conducting polymer (PEDOT:PSS) films possess some extraordinary properties, such as better conductivity and better mechanical strength, and most importantly they change from hydrophilic to hydrophobic.[20] To the best of our knowledge, the electromagnetic properties of MXene interlayered crosslinked PEDOT:PSS films have not been investigated before. In this work, the facile preparation of a $Ti_3C_2T_x$ MXene interlayered crosslinked PEDOT:PSS nanocomposite film was demonstrated and its EMI shielding properties were investigated.

Results and discussion

A schematic of the synthesis of the crosslinked PEDOT:PSS-MXene film is shown in Fig. 1. Details of the $Ti_3C_2T_x$ MXene

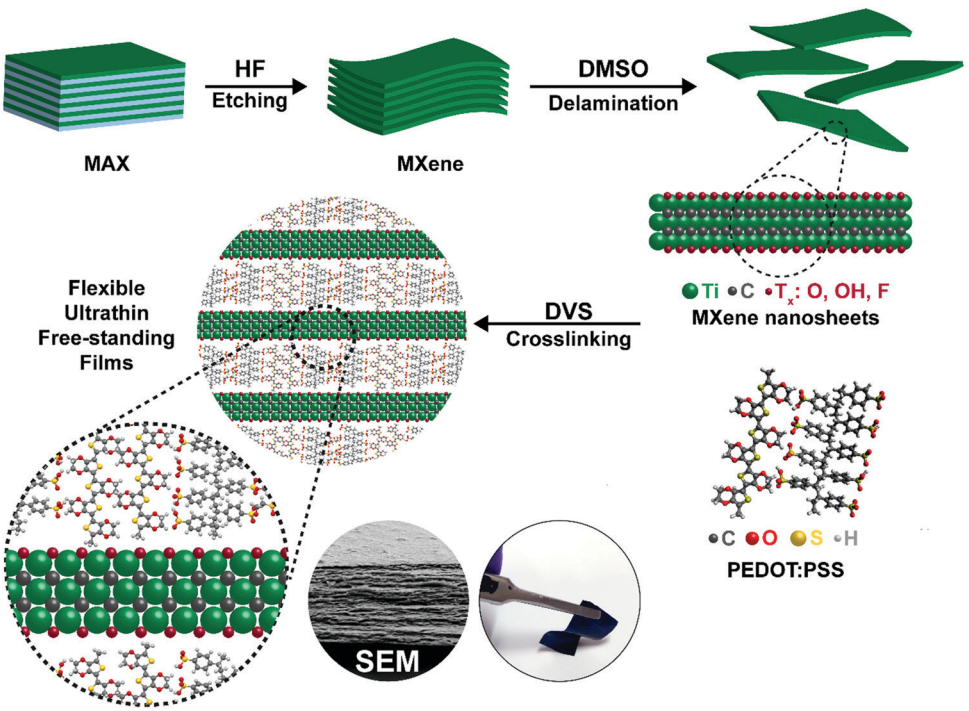

Fig. 1 Schematic of the preparation process of the crosslinked PEDOT:PSS-$Ti_3C_2T_x$ MXene nanocomposite film (the insets show an SEM cross-section image and a photograph of the flexible nanocomposite film).

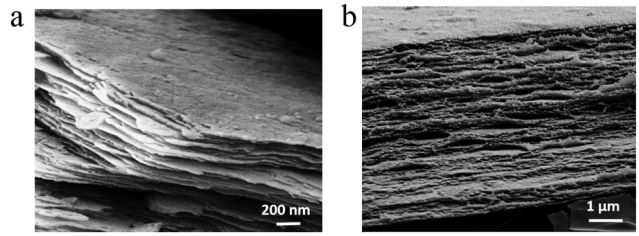

Fig. 2 (a) Surface morphology of the $Ti_3C_2T_x$ MXene and (b) cross-section morphology of the crosslinked PEDOT:PSS-$Ti_3C_2T_x$ MXene nanocomposite (XPM50) film.

synthesis and the crosslinked PEDOT:PSS-$Ti_3C_2T_x$ MXene nanocomposite film preparation are provided in the methods section. The crosslinker used in this work is divinyl sulfone (DVS). As described in the methods section, 10 μL, 25 μL, 50 μL and 100 μL of a $Ti_3C_2T_x$ MXene suspension with a concentration of 0.5 mg mL^{-1} were dispersed into PEDOT:PSS, and the sample films were named XPM10, XPM25, XPM50 and XPM100 respectively.

The surface morphology of the as-synthesized $Ti_3C_2T_x$ MXene is shown in Fig. 2(a). The lateral dimension of the $Ti_3C_2T_x$ MXene is observed to be 1–6 μm with a layered spacing. An optical image of the prepared flexible crosslinked PEDOT:PSS-$Ti_3C_2T_x$ MXene nanocomposite film is shown in Fig. S1 (ESI†). Fig. 2(b) shows the cross-section morphology of the XPM50 nanocomposite film. The cross-section SEM image suggests that the crosslinked PEDOT:PSS is grafted onto the $Ti_3C_2T_x$ MXene and also interconnects the MXene layers (a cross-sectional SEM image of crosslinked PEDOT:PSS is shown in Fig. S2, ESI†).

The FTIR spectrum of the $Ti_3C_2T_x$ MXene interlayered crosslinked PEDOT:PSS nanocomposite film is shown in Fig. 3(a). The FTIR spectrum of the nanocomposite film (Fig. 3(a), XPM50 film) contains peaks corresponding to both the $Ti_3C_2T_x$ MXene and crosslinked PEDOT:PSS. The $Ti_3C_2T_x$ MXene peak at around 475 cm^{-1} corresponds to the C–Cl stretching and the peak at 585 cm^{-1} corresponds to the Ti–O bond.[19] The peak at around 709 cm^{-1} could be assigned to C–H bonds. The C–O stretching is observed near 1259 cm^{-1}.[19] The sulfonate S═O stretching resonances can be seen between 1300 cm^{-1} and 1500 cm^{-1}.[20] The peak at 1536 cm^{-1} corresponds to the aromatic C═C stretching in PEDOT:PSS. The resonance at 2665 cm^{-1} corresponds to the O–H stretching.[20] The X-ray diffraction (XRD) pattern, as shown in Fig. 3(b), further confirms the incorporation of the $Ti_3C_2T_x$ MXene into the crosslinked PEDOT:PSS. XRD peaks corresponding to the $Ti_3C_2T_x$ MXene (Fig. S3, ESI†) as well as PEDOT:PSS were observed for the crosslinked PEDOT:PSS-$Ti_3C_2T_x$ MXene film. The crosslinking mechanism is shown in Fig. 3(c).

The thermogravimetric analysis (TGA) curves are shown in Fig. 4. The sharp weight loss at around 300 °C for the XPM50 nanocomposite film results from the degradation of PEDOT:PSS. The residual weight after this degradation is higher for the XPM50 nanocomposite film owing to the presence of the $Ti_3C_2T_x$ MXene. A gradual weight loss was observed from 500 °C to 750 °C.

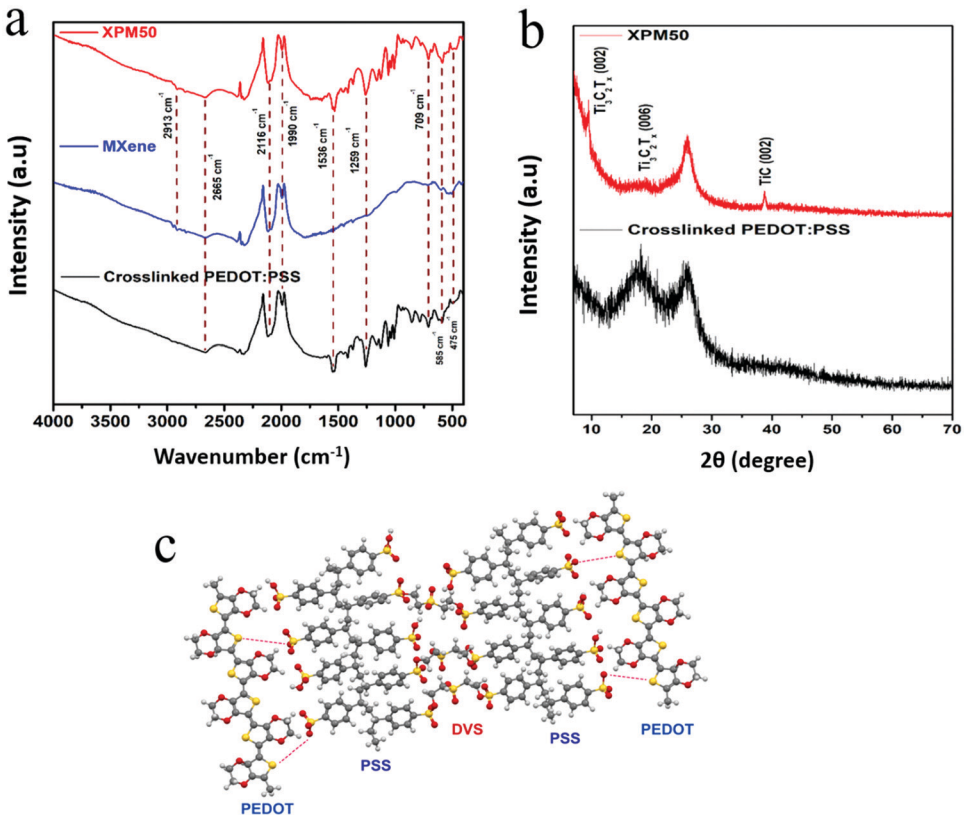

Fig. 3 (a) Comparison of the FTIR spectra of XPM50, the MXene and crosslinked PEDOT:PSS. (b) Comparison of the powder XRD patterns of XPM50 and crosslinked PEDOT:PSS. (c) Crosslinking mechanism.

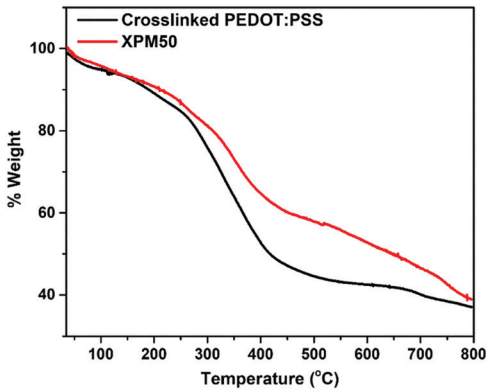

Fig. 4 Thermogravimetric analysis of the XPM50 film and the crosslinked PEDOT:PSS film.

The recorded conductivity of the native PEDOT:PSS film was 0.15 S cm^{-1}. The conductivities of the XPM10, XPM25, XPM50 and XPM100 films were measured to be 325 ± 3, 344 ± 5, 388 ± 2 and 299 ± 2 S cm^{-1} respectively. These results indicate that the influence of the $Ti_3C_2T_x$ MXene enhances the conductivity of the crosslinked PEDOT:PSS film.

To investigate the EMI shielding properties of the crosslinked PEDOT:PSS-$Ti_3C_2T_x$ MXene nanocomposite film, the EMI SE was recorded in the X-band (8.2–12.4 GHz) for three films for each nanocomposite, *viz.* XPM10 (13 ± 0.2 μm), XPM25 (8 ± 0.2 μm), XPM50 (6 ± 0.2 μm) and XPM100 (7 ± 0.2 μm). The recorded EMI SE results of all the nanocomposite films are shown in Fig. 5(a). The 6 ± 1 μm thick XPM50 film exhibits an average EMI SE of ~41 dB (corresponding to 99.999% shielding), comparatively better than the XPM10 (~35 dB), XPM25 (~38 dB) and XPM100 (~40 dB, thickness is slightly higher than that of XPM50) films. The average EMI SE of the pristine PEDOT:PSS film is ~17 dB for a thickness of 38 ± 2 μm (Fig. S4, ESI†). The slight variation observed in the SE value with frequency is believed to be due to multiple reflections.[10] Fig. 5(b) shows the EMI shielding effectiveness due to absorption (SE_A) and reflection (SE_R) of the XPM50 film. It is observed from Fig. 5(b) that the EMI shielding due to absorption is predominant (for the 6 ± 0.2 μm thick XPM50 film with SE_A ~ 37 dB and SE_R ~ 4 dB) for the crosslinked PEDOT:PSS-$Ti_3C_2T_x$ MXene nanocomposite film. The standard electrodynamic simulations carried out with CST-microwave studio (CST-MWS) support the experimental EMI SE data (Fig. 5(c)). The thickness dependent EMI SE (simulated and experimental) of the XPM50 nanocomposite film was also investigated and the trend is depicted in Fig. 5(d).

Conducting polymers are more well known for absorption predominant EMI shielding than metal-based composites.[4,14–16] The proposed mechanism of the excellent absorption predominant EMI shielding properties of the XPM50 film is shown in Fig. 6.

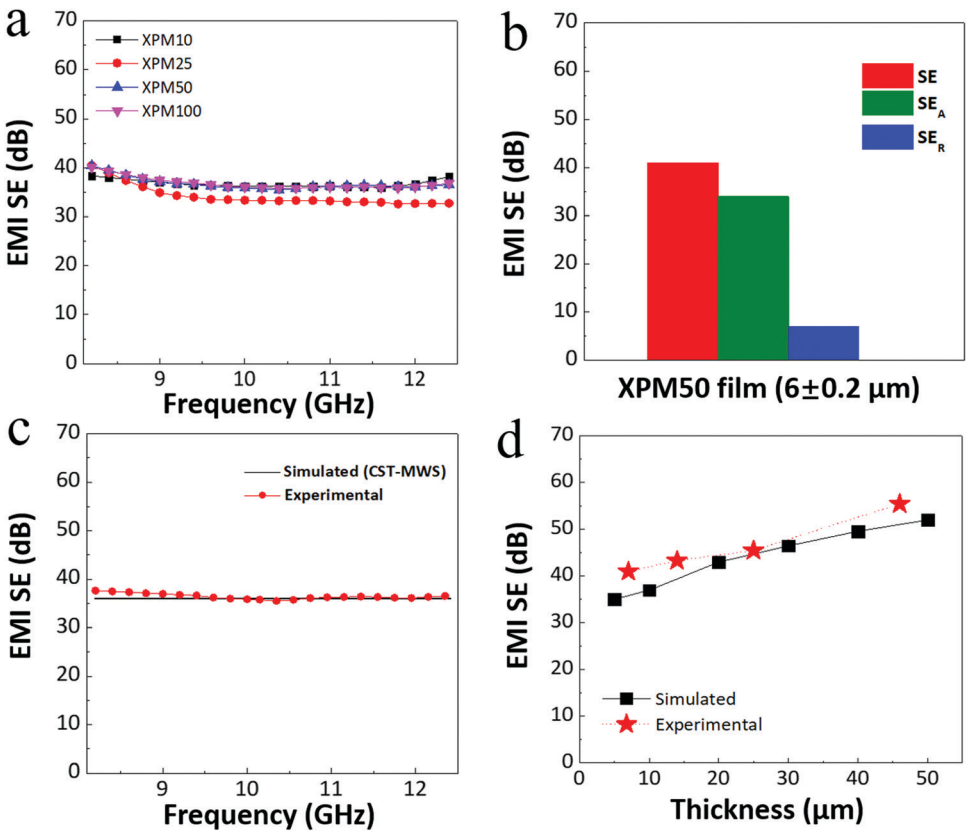

Fig. 5 (a) Recorded EMI SE of different crosslinked PEDOT:PSS-$Ti_3C_2T_x$ MXene nanocomposite films, *viz.* XPM10, XPM25, XPM50 and XPM100 in the X-band (8.2–12.4 GHz). (b) Recorded average EMI SE_A and SE_R values of the XPM50 film for a thickness of 6 ± 0.2 μm. (c) Comparison of the CST-MWS simulated and experimental EMI SE of the XPM50 film. (d) Thickness dependent average EMI SE of the XPM50 film.

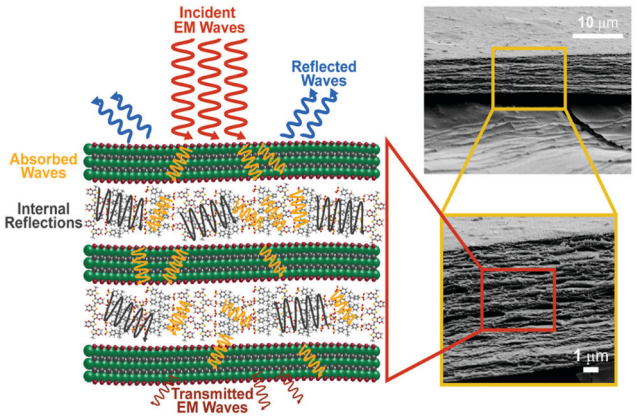

Fig. 6 Schematic of the proposed EMI shielding mechanisms of crosslinked PEDOT:PSS-$Ti_3C_2T_x$ MXene nanocomposite.

The EMI shielding is a material property, and mathematically the SE value can be expressed as Simon's formula,[1] $SE(dB) = 50 + 10\log\left(\frac{\sigma}{f}\right) + 1.7t\sqrt{\sigma f}$. Here, σ = conductivity (S cm^{-1}), f = frequency (MHz), and t = thickness (cm).[1] In addition, the SE value also intrinsically depends on the EMI shield's structure–property relationship.[15–19] When an incident electromagnetic wave (EMW) strikes the crosslinked PEDOT:PSS-MXene nanocomposite, three phenomena occur, *viz.* immediate absorption, reflection and multiple internal reflections. The immediate reflection of the incident EMW from the first layer of XPM is less than in the MXene, as the MXene is grafted onto the crosslinked PEDOT:PSS. The crosslinked PEDOT:PSS contains coagulated particles (Fig. S2, ESI†), which have coarser morphology, and MXene flakes are interconnected through them, increasing the electrical conductivity across the MXene layer. As a result, absorption is predominant and the incident EMW's energy drops.[21–24] As shown in Fig. 6, after passing the first layer, the surviving EMWs are attenuated repeatedly in a similar way through the difficult path.

In addition, multiple internal reflections (Fig. 6) take place within the subsequent layers. After passing the first layer, the surviving EMWs are reflected back and forth between the numerous interlayers of XPM until they are totally absorbed. Moreover, surface terminations on the $Ti_3C_2T_x$ MXene flake, like OH, F and S atoms in the crosslinked bridge, may play an important role in polarisation assisted EMW absorption.[1] Sulfur, fluorine and oxygen atoms, being highly electronegative, may induce dipoles within Ti and the MXene terminating groups. Since they can interact with incident EMWs, this results in polarization loss, which in turn improves the effective absorption predominant shielding.

In the case of the XPM100 film, the maximum amount of the $Ti_3C_2T_x$ MXene was grafted onto the crosslinked PEDOT:PSS, however, the obtained EMI SE was less than that of the XPM50 film. This could be due to many reasons, for example the presence of the large amount of MXene may affect the crosslinking and also the electrical conductivity value (the XPM100 film has a lower conductivity than the XPM50 film), and hence the EMI SE. In addition, agglomeration of the $Ti_3C_2T_x$ MXene could happen in the case of the XPM100 film, which hinders the formation of an efficient network. As a result, the energy drop and EM attenuation do not take place efficiently in the XPM100 film, affecting the EMI SE.

It should be noted that for the ~6 μm thick XPM50 film, the recorded EMI SE was ~41 dB and the corresponding SE_A value was ~37 dB. The previously reported maximum EMI SE of a 9 μm thick PEDOT:PSS-MXene film was ~42 dB and the corresponding SE_A and SE_R values were ~30 dB and ~12 dB, respectively.[19] Thus, this indicates that the crosslinked PEDOT:PSS-MXene film has a better absorption predominant EMI shielding capability at lower thickness as compared to the PEDOT:PSS-MXene film. The absolute EMI shielding effectiveness, *i.e.* specific EMI SE (SSE)/thickness is the most useful quantity for investigating ultra-thin lightweight EMI shielding materials as it intrinsically depends on the EMI SE, the density of the shield and the thickness (calculation details are provided in the ESI†).[1,5,19] The absolute EMI SE value of the XPM50 film is 89 924 dB cm^2 g^{-1} which is more than four times higher than that of the PEDOT:PSS-MXene film (19 497.8 dB cm^2 g^{-1}). A comparison of the absolute EMI SE value of the XPM50 film with those of various other shielding materials such as carbon foam, MXene foam, solid carbon, solid metal, MXene, PEDOT:PSS and crosslinked PEDOT:PSS is shown in Fig. 7 (a comprehensive literature

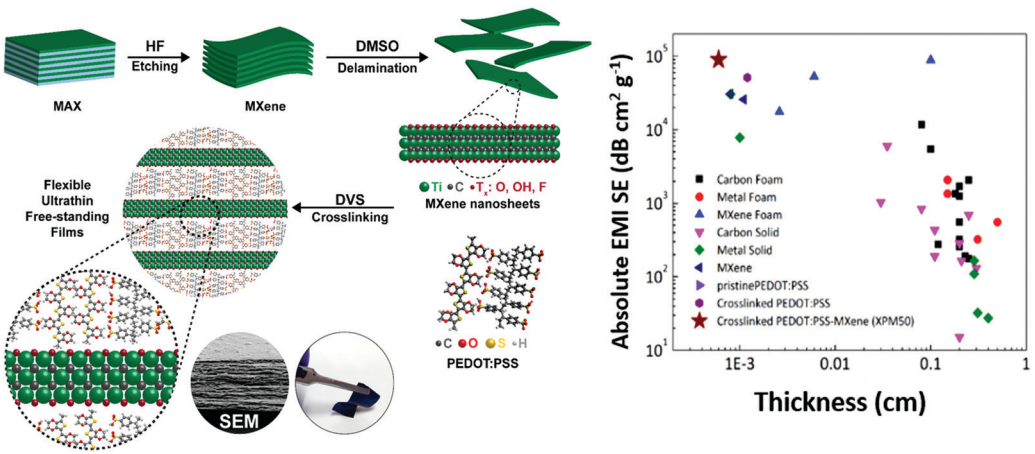

Fig. 7 Comparison of the absolute EMI SE of the XPM50 film with previous literature (ESI†).

survey is tabulated in Table S1, ESI†). Compared to other very recently developed EMI shielding composite materials such as epoxy-MXene,[11] epoxy-Fe_3O_4 decorated CNT/reduced graphene oxide,[8] the XPM50 film has better EMI shielding (absorption predominant) properties at a minimum thickness. Unlike the PEDOT:PSS-MXene film, the XPM50 film is water-insoluble (Fig. S5, video link is provided in the ESI†) with better absorption predominant EMI shielding and absolute EMI shielding properties at lower thickness. Moreover, the XPM50 film also fulfils many commercial requirements such as the preference for lightweight, coatable, water-insoluble and inexpensive materials.

Conclusions

The facile preparation of a water-insoluble crosslinked PEDOT:PSS-$Ti_3C_2T_x$ MXene (XPM) nanocomposite film was demonstrated and its EMI shielding properties were investigated in the X-band (8.2–12.4 GHz). The solution processed, optimized thin XPM50 film (6 ± 0.2 μm) exhibits excellent EMI shielding properties (99.999%). The EMI shielding due to absorption is intrinsically predominant. The mechanism of the EMI shielding properties of the XPM film was studied in detail. The absolute EMI SE of the XPM50 film was calculated to be 89 924 dB cm^2 g^{-1}, which is over sixty thousand higher than that of the pristine $Ti_3C_2T_x$ MXene. The free-standing thin XPM50 film with very high absolute EMI SE is clearly a game changer in ultra-lightweight EMI shielding materials.

Methods

All chemicals were used as purchased unless stated otherwise. Titanium aluminium carbide was obtained from Forsam chemicals, China. Pvt. Lt. Hydrofluoric (HF) acid was purchased from Thomas Baker. Clevios PH1000 was procured from Heraeus and is a dispersion of PEDOT:PSS with a solid content of 1–1.3% as per the datasheet. Divinyl sulfone (DVS) was obtained from Sigma-Aldrich and is a colorless liquid with a density of 1.177 g mL^{-1}.

MXene synthesis

In a typical MXene synthesis, 20 mL 10 wt% HF solution was prepared with deionized water in a 100 mL propylene plastic vial. 0.5 g of Ti_3AlC_2 was gradually added to this etchant solution, with constant stirring. The reaction was continued at 35 ± 2 °C for 24 h. The reaction mixture was then centrifuged at 3500 rpm for 5 min. The supernatant was discarded and the sediment was repeatedly washed with DI water until the pH of the supernatant was ~6. Multiple layers of the obtained $Ti_3C_2T_x$ were exfoliated using dimethyl sulfoxide (DMSO). The obtained clay-like sediment was re-dispersed in 20 mL DMSO and stirred at room temperature for 18 h. The exfoliated $Ti_3C_2T_x$ was washed with DI water several times, to remove any traces of DMSO. The sediment was then dried in air to obtain dark $Ti_3C_2T_x$ powder.

Film preparation

Various amounts of MXene dispersed in solution (0.5 mg mL^{-1} in DI water), namely 10 μL, 25 μL, 50 μL, and 100 μL, were mixed with 5 mL PH1000 and stirred for 2 hours. 5 vol% DVS solution was added to this mixture and stirring was continued for another 20 min. Freshly prepared solutions were used for film casting over PET substrates. After annealing at 50 ± 5 °C for 1 h, the films were extracted from the substrate and named XPM10, XPM25, XPM50, and XPM100 for 10 μL, 25 μL, 50 μL, and 100 μL loading respectively.

Characterization

The surface morphologies of the synthesized composites and films were examined using a field emission scanning electron microscope (FESEM, Carl Zeiss, samples were coated over carbon tape). The thickness of the prepared films was measured using a Dektak contact mode profilometer and cross-sectional FESEM. The conductivity of the as-prepared nanocomposite films was measured using the 4-point probe van der Pauw method. The measurements were carried out using an ATT PM5 thermal chuck coupled with an Agilent Device Analyser B1500, and Easy EXPERT software was used for the calculations. Silver paste was used for better contact between the needle probes and the sample. FTIR spectroscopy was carried out on a Bruker TENSOR II FTIR instrument using the attenuated total reflectance (ATR) mode. X-ray diffraction experiments were performed on a Rigaku Smart Lab X-ray diffractometer. Thermogravimetric analysis was carried out using a TGA analyzer (TA Q50) at a ramp rate of 10 °C min^{-1} in a nitrogen atmosphere. The EMI SE values of the prepared composites were measured by using a vector network analyzer (VNA, Agilent N5230A) through the industrial standard waveguide method. The standard complete two-port calibration of the VNA (thru-reflect-line or TRL) was performed in the X-band (8.2–12.4 GHz) before the measurements. Details of the EMI shielding measurements and electrodynamic simulation using CST-Microwave studio are provided in the ESI.†

Conflicts of interest

The authors declare no competing interests.

Acknowledgements

Authors greatefully acknowledge the Prof. K. J. Vinoy, Department of Electrical and Communication Engineering, IISc, India for providing the VNA facility and help for the EMI shielding measurements. PCR would like to acknowledge the Government of India, Ministry of Defence Aeronautics Research & Development Board (ARDB/01/2031900/M/I) for financial support of this work. This work was also supported by the Guangdong Basic and Applied Basic Research Foundation – 2019A1515012056.

References

1 F. Shahzad, M. Alhabeb, C. B. Hatter, B. Anasori, S. Man Hong, C. M. Koo and Y. Gogotsi, *Science*, 2016, **353**, 1137.
2 D. X. Yan, H. Pang, B. Li, R. Vajtai, L. Xu, P. G. Ren, J. H. Wang and Z. M. Li, *Adv. Funct. Mater.*, 2015, **25**, 559.

3 J. Liu, H. Bin Zhang, R. Sun, Y. Liu, Z. Liu, A. Zhou and Z. Z. Yu, *Adv. Mater.*, 2017, **29**, 1702367, DOI: 10.1002/adma.201702367.
4 P. J. Bora, A. G. Anil, K. J. Vinoy and P. C. Ramamurthy, *Adv. Mater. Interfaces*, 2019, 1901353.
5 P. J. Bora, G. Lakhani, P. C. Ramamurthy and G. Madras, *RSC Adv.*, 2016, **6**, 79058.
6 L. X. Liu, W. Chen, H. Bin Zhang, Q. W. Wang, F. Guan and Z. Z. Yu, *Adv. Funct. Mater.*, 2019, **29**, 1905197.
7 R. Bian, G. He, W. Zhi, S. Xiang, T. Wang and D. Cai, *J. Mater. Chem. C*, 2019, **7**, 474–478.
8 C. Liang, P. Song, A. Ma, X. Shi, H. Gu, L. Wang, H. Qiu, J. Kong and J. Gu, *Compos. Sci. Technol.*, 2019, **181**, 107683, DOI: 10.1016/j.compscitech.2019.107683.
9 P. Song, C. Liang, L. Wang, H. Qiu, H. Gu, J. Kong and J. Gu, *Compos. Sci. Technol.*, 2019, **181**, 107698, DOI: 10.1016/j.compscitech.2019.107698.
10 Z. Shen and J. Feng, *ACS Sustainable Chem. Eng.*, 2019, **7**, 6259–6266, DOI: 10.1021/acssuschemeng.8b06661.
11 L. Wang, L. Chen, P. Song, C. Liang, Y. Lu, H. Qiu, Y. Zhang, J. Kong and J. Gu, *Composites, Part B*, 2019, **171**, 111–118, DOI: 10.1016/j.compositesb.2019.04.050.
12 P. Song, H. Qiu, L. Wang, X. Liu, Y. Zhang, J. Zhang, J. Kong and J. Gu, *Sustainable Mater. Technol.*, 2020, **24**, e00153, DOI: 10.1016/j.susmat.2020.e00153.
13 X. Zhang, H. Wang, R. Hu, C. Huang, W. Zhong, L. Pan, Y. Feng, T. Qiu, C. (John) Zhang and J. Yang, *Appl. Surf. Sci.*, 2019, **484**, 383–391, DOI: 10.1016/j.apsusc.2019.03.264.
14 P. J. Bora, N. Mallik, P. C. Ramamurthy, Kishore and G. Madras, *Composites, Part B*, 2016, **106**, 224–233, DOI: 10.1016/j.compositesb.2016.09.035.
15 P. J. Bora, K. J. Vinoy, P. C. Ramamurthy, Kishore and G. Madras, *Compos. Commun.*, 2017, **4**, 37–42, DOI: 10.1016/j.coco.2017.04.002.
16 P. J. Bora, I. Azeem, K. J. Vinoy, P. C. Ramamurthy and G. Madras, *ACS Omega*, 2018, **3**(12), 16542–16548, DOI: 10.1021/acsomega.8b02037.
17 Y. Zhang, L. Wang, J. Zhang, P. Song, Z. Xiao, C. Liang, H. Qiu, J. Kong and J. Gu, *Compos. Sci. Technol.*, 2019, **183**, 107833, DOI: 10.1016/j.compscitech.2019.107833.
18 P. Li, D. Du, L. Guo, Y. Guo and J. Ouyang, *J. Mater. Chem. C*, 2016, **4**, 6525.
19 R. Liu, M. Miao, Y. Li, J. Zhang, S. Cao and X. Feng, *ACS Appl. Mater. Interfaces*, 2018, **10**, 44787–44795, DOI: 10.1021/acsami.8b18347.
20 D. Mantione, I. Del Agua, W. Schaafsma, M. Elmahmoudy, I. Uguz, A. Sanchez-Sanchez, H. Sardon, B. Castro, G. G. Malliaras and D. Mecerreyes, *ACS Appl. Mater. Interfaces*, 2017, **9**(21), 18254–18262, DOI: 10.1021/acsami.7b02296.
21 B. Shen, W. Zhai and W. Zheng, *Adv. Funct. Mater.*, 2014, **24**, 4542–4548.
22 P. Kumar, F. Shahzad, S. Yu, S. M. Hong, Y.-H. Kim and C. M. Koo, *Carbon*, 2015, **94**, 494–500.
23 B. Shen, Y. Li, D. Yi, W. Zhai, X. Wei and W. Zheng, *Carbon*, 2016, **102**, 154–160.
24 F. Fang, Y.-Q. Li, H.-M. Xiao, N. Hu and S.-Y. Fu, *J. Mater. Chem. C*, 2016, **4**, 4193–4203.